WPPFC-CPR(18) 18752

A Weckmann et al.

Whole-machine high-Z migration modelling and parameter studies with ASCOT code

Preprint of Paper to be submitted for publication in Proceeding of 23rd International Conference on Plasma Surface Interactions in Controlled Fusion Devices (PSI-23)

This work has been carried out within the framework of the EUROfusion Consortium and has received funding from the Euratom research and training programme 2014-2018 under grant agreement No 633053. The views and opinions expressed herein do not necessarily reflect those of the European Commission.

Physics affecting heavy impurity migration in tokamaks: benchmarking test-ion code ASCOT against TEXTOR tracer experiment

A. Weckmann[1], T. Kurki-Suonio[2], K. Särkimäki[2], J. Romanzanov[3], A. Kirschner[3], A. Hakola[4], M. Airila[4], A. Kreter[3], S. Brezinsek[3]

[1] *Department of Fusion Plasma Physics, KTH Royal Institute of Technology, 10044 Stockholm, Sweden*

[2] *Department of Applied Physics, Aalto University, 00076 Aalto, Finland*

[3] *Forschungszentrum Jülich GmbH, Institut für Energie- und Klimaforschung – Plasmaphysik, 52425 Jülich, Germany*

[4] *VTT Technical Research Centre of Finland Ltd., 02044 VTT, Finland*

ABSTRACT

Erosion, transport and deposition of wall impurities are major concerns in future magnetic fusion devices, both from the perspective of the fusion plasma and the machine wall. An extensive study on molybdenum transport and deposition performed in the TEXTOR tokamak yielded a detailed deposition map that is ideal for benchmark deposition studies. A qualitative benchmark is attempted in this article with the ASCOT code.
We set up a full 3D model of the TEXTOR tokamak and studied the influence of different physical mechanisms and their strengths on molybdenum deposition patterns on the simulated plasma-facing components: atomic processes, Coulomb collisions, scrape-off layer (SOL) profiles, source distribution, marker starting energy, radial electric field strength, SOL flow and toroidal plasma rotation. The outcome comprises 13 simulations, each with 100 000 markers.
The findings are:

- Toroidal plasma movement, either within the LCFS or as SOL flow, is negligible.
- SOL profile and marker starting energy have modest impact on deposition.
- Source distribution has a large impact in combination with radial electric field profiles.
- The $\vec{E} \times \vec{B}$ drift has the highest impact on the deposition profiles.

INTRODUCTION

In fusion machines – nowadays in research devices and even more so in future reactors – interactions between fusion plasma and wall components will cause erosion, transport of eroded material into the plasma, and deposition of the material on other wall components. This plasma-wall interaction (PWI) and the resulting transport of impurity particles in the plasma leads to undesirable effects both for plasma-facing components (PFCs) and the plasma itself. Understanding PWI and transport has thus become a major goal within fusion research which is addressed both experimentally and by modelling. Increased experimental and computational capabilities have led to a combination of both approaches where usually a transport experiment is conducted and later modelled *in silico* to benchmark the applied code or to better understand experimental results.

This work is based on combined effort where a molybdenum tracer experiment was conducted in the tokamak TEXTOR which was dismantled directly thereafter and had its PFCs analysed in order to map the tracer deposition patterns [1] [2]. The experimental results were thus a perfect opportunity for modelling because deposition data from the whole machine was available. Furthermore, the tracer experiment itself had been conducted in TEXTOR under well-established standard NBI conditions.
Subsequent modelling on both local and global scale was undertaken with ERO [3] and ASCOT for code benchmarking and understanding the experimentally obtained deposition patterns. In this article we will focus on the exploitation of the ASCOT model.

ASCOT is a Monte Carlo code capable of modelling an entire tokamak with full 3D wall structures and magnetic fields, tracing either the guiding centres or full gyro orbits of impurity particles in a pre-defined background plasma [4]. Plasma flows, drifts, Coulomb collisions and atomic processes can be simulated in order to cover most relevant processes for impurity transport.
We attempted to reproduce the global molybdenum deposition patterns found on the PFCs of TEXTOR by using first principle physics only, i.e. no tuning of free parameters to reproduce the measured deposition patterns. Full gyro orbits were simulated, i.e. curvature and grad(B) drifts were inherent due to the simulated 3D magnetic field. The attempt to reproduce experimental results yielded very interesting insights into the physics of impurity transport.
In this article we will explore the ASCOT model of the very last TEXTOR molybdenum tracer experiment, show the impact of different physical mechanisms that can be toggled on and off at will in a computer simulation, and evaluate the impact of different physical mechanisms: atomic processes, Coulomb collisions, scrape-off layer (SOL) profiles, marker[1] source distributions, marker starting energies, radial electric field strength, SOL flow and toroidal plasma rotation. The aim is to investigate the importance – or unimportance – of different plasma physical mechanisms on modelled deposition patterns and to illustrate where transport models must be detailed, and where using simpler parametrisation is sufficient without compromising the simulation outcome.
PWI including sputtering, re-erosion or reflection is important for formation of deposition profiles. However, those effects are not supported by ASCOT and will not be treated here. Furthermore, the focus is on qualitative deposition pattern simulation – no quantitative analysis was possible with the present version of ASCOT (ASCOT4 [4]).

METHODS

The tracer experiment in TEXTOR and its evaluation have been described in depth elsewhere [1] [2] [5]. For convenience, a short outline is given here. The investigated tokamak was a carbon limiter machine with major radius of 1.75 m and minor radius of 0.46 m. Experimental conditions are given in Table 1. Only neutral beam injection (NBI) of 1.7 MW in co-direction was used for auxiliary heating. Injected amounts of tracers were $5.7 \cdot 10^{20}$ of MoF_6 and $5.3 \cdot 10^{21}$ of $^{15}N_2$. Directly after the experiment, TEXTOR was decommissioned, the PFCs dismantled and shipped to the Tandem Laboratory at Uppsala University, Sweden, for subsequent ion beam analysis (IBA) to obtain the amount of deposited tracers on the different PFC tiles. Overall, 140 tiles from the ALT-II main limiter and the inner bumper limiter (IBL) throughout the whole machine were

[1] In this paper, “tracer” denotes molybdenum atoms/ions injected in the real experiment whereas “marker” denotes simulated molybdenum in ASCOT.

analysed. The focus of the ASCOT study was on the molybdenum transport and deposition.

ASCOT stands for Accelerated Simulation of Charged particle Orbits in Tori and has been developed for more than 20 years [6]. It is a Monte Carlo code, solving for the Fokker-Planck equation by calculating the movement of minority species through phase space, including drifts, collisions and background plasma flow [4]. These markers can be followed either along their guiding centres or with their full gyro motion, with the latter one using either a fourth-order Runge-Kutta method or a modified leap-frog method to solve the equations of motion [7]. Rates for atomic interactions – neutralisation and ionisation – are included from the ADAS database [8].
The geometry is a 3D model of TEXTOR, including all PFCs and the injection limiter (test limiter). The simulation environment is illustrated in Figure 1. Both magnetic field and background plasma are fixed and given as input. The magnetic topology was extracted from EFIT output for the experimental discharges. The background plasma was obtained from values of previous measurements with comparable engineering parameters, fitting parabolic profiles to experimental flow velocity, temperature and density values. It was furthermore assumed that the plasma is made of pure deuterium, quasi-neutral and hence obeys $n_e = n_i$. The kinetic profiles are given in Figure 2.
The influence of the following physical mechanisms was studied:

- Atomic processes, i.e. ionisation and recombination (on/off),
- Coulomb collisions (on/off),
- Radial electric field in whole simulation volume (on/off),
- Bulk plasma rotation (on/off),
- Source distribution (point source at r = 48 cm, radially extended source, see Fig. 2f)
- Marker starting energy (1 eV, 10 eV)
- Strength of SOL radial electric potential (0, T_e, $3T_e$)
- Strength of SOL toroidal velocity (0, sound speed)
- SOL profile (exponential, linear)

For atomic processes, the cross-sections are obtained from the ADAS data base [8]. Coulomb collision cross-sections are derived from the Fokker-Planck equation, using binomially distributed Monte Carlo operators. The radial electric field is a fourth order polynomial fit to experimental data obtained in [9]. Parabolic fits were used for bulk plasma rotation to data in [9] [10], for ion and electron temperatures to data in [9] [10] [11] and [11] [12], respectively, and for electron and ion density to data in [11] [13] [14]. Used formulas are listed in Table 2. The source was either a point source at r = 48 cm (i.e. 2 cm outside the LCFS and 1.3 cm above the gas inlet), or a radially extended source consisting of 100 000 markers, fitted with weight factors according to a spectroscopically obtained MoI profile during MoF_6 injection [5]. The marker starting energy is either 1 or 10 eV since the dissociation energy of MoF_6 is ca. 5 eV for each F atom, whereof only a fraction is transferred to the Mo atom (or the Mo atom containing molecule fragment) [15]. The electric potential in the SOL was set equal to the electron temperature with and without sheath potential drop, i.e. $3T_e$ and $1T_e$, respectively. The former case leads to an exaggeration since the sheath potential drop hardly influences the particle trajectory on the last few Debye lengths away from the target; it was therefore used as a “worst case” scenario. As toroidal velocity in the SOL the sound speed c_s was used to estimate the maximum possible influence of plasma flow along field lines towards the targets. Finally, two kinds of SOL profile shapes for T_e and n_e were used to estimate the impact of SOL

profile shape on the marker transport: a realistic one based on experimental values in [3] [16], with T_e(LCFS) = 30 eV (e-folding length: 40 mm) and n_e(LCFS) = $5 \cdot 10^{18}$ m^{-3} (e-folding length: 30 mm), and a linear one with T_e(LCFS) and n_e(LCFS) decreasing from their LCFS values down to almost zero[2] at r = 56 cm.
For a direct comparison of experimental [5] and simulated deposition profiles, the final marker positions in the ASCOT output were mapped in the same way as the experimental values. The approach is described in detail in [5].

RESULTS AND DISCUSSIONS

For easy identification, the different cases are labelled with Latin numbers (I) – (XIII). An overview of the simulations and the parameters used is given in Table 3.

Gyration, atomic processes and Coulomb collision

The first Simulation (I) was done with markers released from a point source, starting at 1 eV and only following the field lines. No other physics was included but the Gyro motion. The markers get lost quickly on the test limiter, with a circular deposition profile of 0.5 mm in width. This profile is due to the gyro motion. In the other direction, the field line ends below the IBL and no deposition is seen globally.
Including atomic processes only in Simulation (II), the local deposition profile is broadened on the test limiter to a few millimetres due to cross-field movement of neutralised markers, but again no global deposition takes place. With Coulomb collisions only, in Simulation (III) the situation is the same, with broadening of the local deposition profile due to cross-field diffusion by collision.
When both atomic processes and Coulomb collision are combined in Simulation (IV), we see global deposition for the first time. This deposition takes place on the IBL bottom tiles since markers, which otherwise would have ended up *below* the IBL tiles, now can traverse the magnetic field lines quickly enough by diffusion and neutralisation in order to enter field lines ending *on* the IBL tiles.

Central plasma rotation and electric field

After atomic processes and Coulomb collisions, we investigated the impact of radial electric field E(r), as found experimentally in [9], and plasma rotation, as found experimentally in [9] [10] (both inside and outside LCFS). The profiles are given in Fig. 2. The following cases were treated: toroidal rotation only (V), radial electric field only (VI), both rotation and field (VII).
The rotation of the centre plasma had virtually no effect on the deposition profile, see Figure 3. This is because the most markers stay well outside the region of strong toroidal rotation. The amount of markers which go beyond the LCFS is small compared to the amount staying in the SOL.
Introducing the electric field (VI) makes a huge difference and immediately brings the global deposition maximum closer to the injection. The $\vec{E} \times \vec{B}$ drift causes a fast poloidal movement towards the high field side, and the markers intercept the IBL earlier than before where movement along the magnetic field clearly dominated, see Figure 4.
However, the central plasma rotation still has very low influence on the deposition (VII).

[2] Actually, the values were not exactly zero at the vessel wall because that would have led to divergence in the Coulomb collision operator. Instead, both values were set to 0,1 eV and 10^{13} m^{-3} which is negligible compared to the LCFS values.

Source distribution and marker starting energy

The molybdenum in the real experiment was injected in the form of MoF_6. The molybdenum source is not a point source but rather a three-dimensional cloud of particles (not a jet!). The molybdenum-containing particle distribution can be approximated to first order by MoI line radiation, and has been successfully reproduced already with ERO modelling [3]. In this work, we approximate the extended source by a radial distribution with weighted markers, see Fig. 2f.
The molybdenum-containing deposits can be formed both by molybdenum from completely dissociated molecules, or from molecule fragments containing molybdenum. The dissociation energy for each step is ca. 5 eV [15], where the kinetic energy from dissociation alone can range from 0,5 eV ($MoF_6 \rightarrow MoF_5 + F$) to 3,7 eV ($MoF_6 \rightarrow \ldots \rightarrow 6F + Mo$). Different processes (Coulomb collisions, radiation absorption, ionisation) can lead to higher kinetic energy.
We therefore explored the impact of a radially extended source and the marker starting energy on the deposition pattern. Introducing the extended source led to a slightly stronger spreading on the bottom IBL in clockwise direction, compare Fig. 4 (VII) and Fig. 5 (VIII). With a radially extended source, more than one magnetic field line is populated with markers, leading to broadened deposition profiles due to slightly different intersection points between different populated field lines and PFCs in the SOL. However, this is only the case for a strong electric field, resulting from a potential of $3T_e$ over the entire SOL. For a more realistic case given by $1T_e$ the situation changes, as will be seen later. Concerning starting energy, we find only modest influence between 1 eV (VIII) and 10 eV (IX), see Figure 5. The deposition maximum is shifted a few degrees in toroidal direction since the ratio between the $\vec{E} \times \vec{B}$ drift velocity (radial electric field was always active) and thermal velocity along field lines is different for different starting energies.

The SOL potentials have been exaggerated for clear visibility of effect, leading to a three times too strong electric field. When changing to a more realistic electric field (X) the deposition on the IBL moves toroidally further away, see Fig. 6 (X): about 60° as compared to 20° with three times too strong field (Fig. 5). Still no deposition on the ALT-II limiter is visible. When extending the radial source to 44 cm (X-b; otherwise it terminates at 46,5 cm, see Fig. 2f) we see deposition on the ALT-II limiter for the first time, see Fig. 6 (X-b). The markers now start also from positions *inside* the LCFS and are therefore more likely to be deposited on the ALT-II limiter top. As will be seen in the next section, this is not the only possibility to get deposition on the ALT-II.

SOL flow and profiles: potential, temperature, density

Especially for tracer experiments with source in the SOL, the properties of the SOL are very important for particle transport. However, implementing the details of the SOL – e.g. flows, potential, temperature and density profiles – can be challenging, either due to the lack of experimental data or limited possibilities of implementing detailed profiles in the simulation. This is also the case for ASCOT: there is no plasma sheath in front of the PFCs, and SOL flow as function of distance from the PFC is difficult to implement.
In the recent two simulations (X, X-b) we set the SOL potential to $1T_e$, which is more realistic than the formerly used $3T_e$. This reduces the $\vec{E} \times \vec{B}$ drift by a factor of 3.
Next we implemented a toroidal velocity in the SOL with sound speed c_s, in order to investigate the impact of flow velocity on the marker deposition for a “worst case” scenario (XI). For direct comparison with previous cases, and for emphasising the SOL

transport, we again set the radial source as in Fig. 2f, i.e. terminating at r = 46,5 cm. The electric field was deactivated for case (XI) in order have a direct comparison to simulations (IV) and (V) with point source and SOL flow equal zero for both cases. As in the case for central plasma velocity, no major impact can be detected. The deposition on the IBL is hardly affected by the SOL flow, see Fig. 7 (XI). On the other hand, switching from a point source to a radial source, in combination with deactivating the electric field, leads to deposition on the ALT-II limiter because traceable amounts of markers now can cross the LCFS before being deposited on the IBL. The deposition takes place where it would be expected with a safety factor of about 4: the lower edge of the ALT-II blades is 30° away poloidally, leading to a toroidal distance of 120° for deposition, which is observed in the simulation. Notably, this is the same position as in case (X-b) *with* electric field and extended source.
When activating the electric field again, this time with a potential of $1T_e$, in combination with the SOL flow (XII), the deposition on the IBL is the same as in case (X) (similar to XII, just without SOL flow) while the deposition on the ALT-II limiter decreases drastically, yet it stays at the same place as before, see Figure 7 (XII). The main difference between (XII) and (X-b) is the source extension: 46,5 cm versus 44 cm, respectively. This indicates that the radial electric field and the radial source are the main drivers behind position and quantity of deposited markers, not so much the toroidal plasma movement.

When changing the exponential profile of the SOL to a linear one (XIII) while keeping everything else the same as in Simulation (XII), a slight change appears in deposited quantities: the deposition on ALT-II increases while the deposition on the IBL decreases, see Fig. 8 (XIII). The qualitative picture remains unchanged as compared to Simulation (XII). Hence, a linear SOL increases chances for markers to cross the LCFS, probably due to higher Coulomb collision probability than in the exponential case ($\nu_{ei} \propto n/T^{3/2}$, hence a flatter increase in T yields higher ν_{ei}, see e.g. [17]).

CONCLUSION

We used the TEXTOR MoF_6 marker experiment as a setting for extensive ASCOT simulations, studying the importance of various physical mechanisms. The following conclusions are drawn.

- Toroidal plasma movement, either in central plasma due to NBI or in the SOL due to flow towards the PFCs, has very small influence on high-Z marker deposition.
- The $\vec{E} \times \vec{B}$ drift is one of the most important parameters for global marker transport, and hence exact knowledge of radial electric field profiles is needed for proper impurity transport code benchmarking.
- The source distribution is another important parameter, yet its impact on simulation results depends on the strength of the radial electric field.
- Marker starting energy has a modest influence on deposition. For detailed studies one therefore needs to simulate also the dissociation of molecules. For rather coarse assessments, approximations might be feasible.
- While changing the SOL profile does not change the qualitative picture, the deposition efficiencies are notably altered.

Finally, when comparing the qualitative results with experimentally obtained results, see Figure 8, the closest match is obtained by Simulations (VI) – (VIII), albeit with three

times too strong electric field. This illustrates that the closest match between experiment and simulation is not necessarily obtained by the most realistic set of simulation parameters. The most realistic set of parameters investigated in ASCOT was in Simulation case (X-b). Still, substantial features of the experimental deposition patterns could not be obtained: deposition on the ALT-II limiter next to the gas inlet, and deposition on top of the IBL. This indicates the importance of PWI effects neglected in the present ASCOT simulations. We therefore encourage benchmarking and parameter studies with other 3D codes including PWI processes, e.g. ERO 2.0.

ACKNOWLEDGEMENTS

This work has been carried out within the framework of the EUROfusion Consortium and has received funding from the Euratom research and training programme 2014-2018 under grant agreement No 633053. The views and opinions expressed herein do not necessarily reflect those of the European Commission.

Figure 1: a) ASCOT simulation environment of the TEXTOR tokamak, displaying high local deposition on the injection limiter (Limiter Lock 1). The main limiter (ALT-II) is to the right,

the inner bumper limiter (IBL) is to the left. The simulation volume is limited otherwise by the TEXTOR liner. – b) Dummy plot of the PFC surfaces for orientation purposes. The white arrow points in the direction of the toroidal plasma flow, the red arrow in the direction of the magnetic field, and the yellow arrow in the direction of the $\vec{E} \times \vec{B}$ drift outside the LCFS (opposite direction applies inside the LCFS). The IBL top is the inner rim of the full circle.

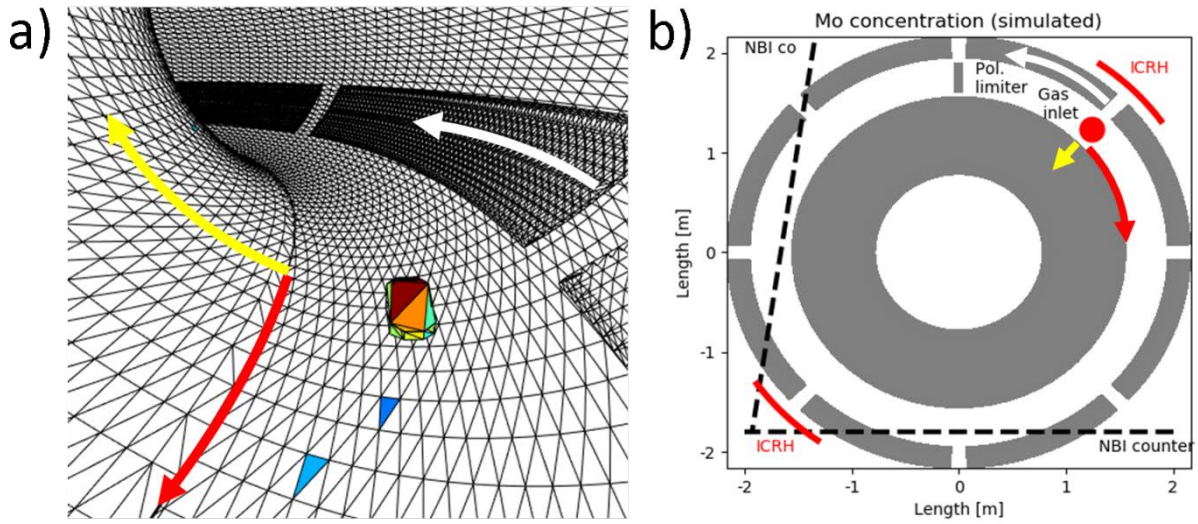

Figure 2: radial profiles of the input plasma – a) electron temperature, b) ion temperature, c) electron density, d) toroidal velocity, e) electric field, f) radial source.

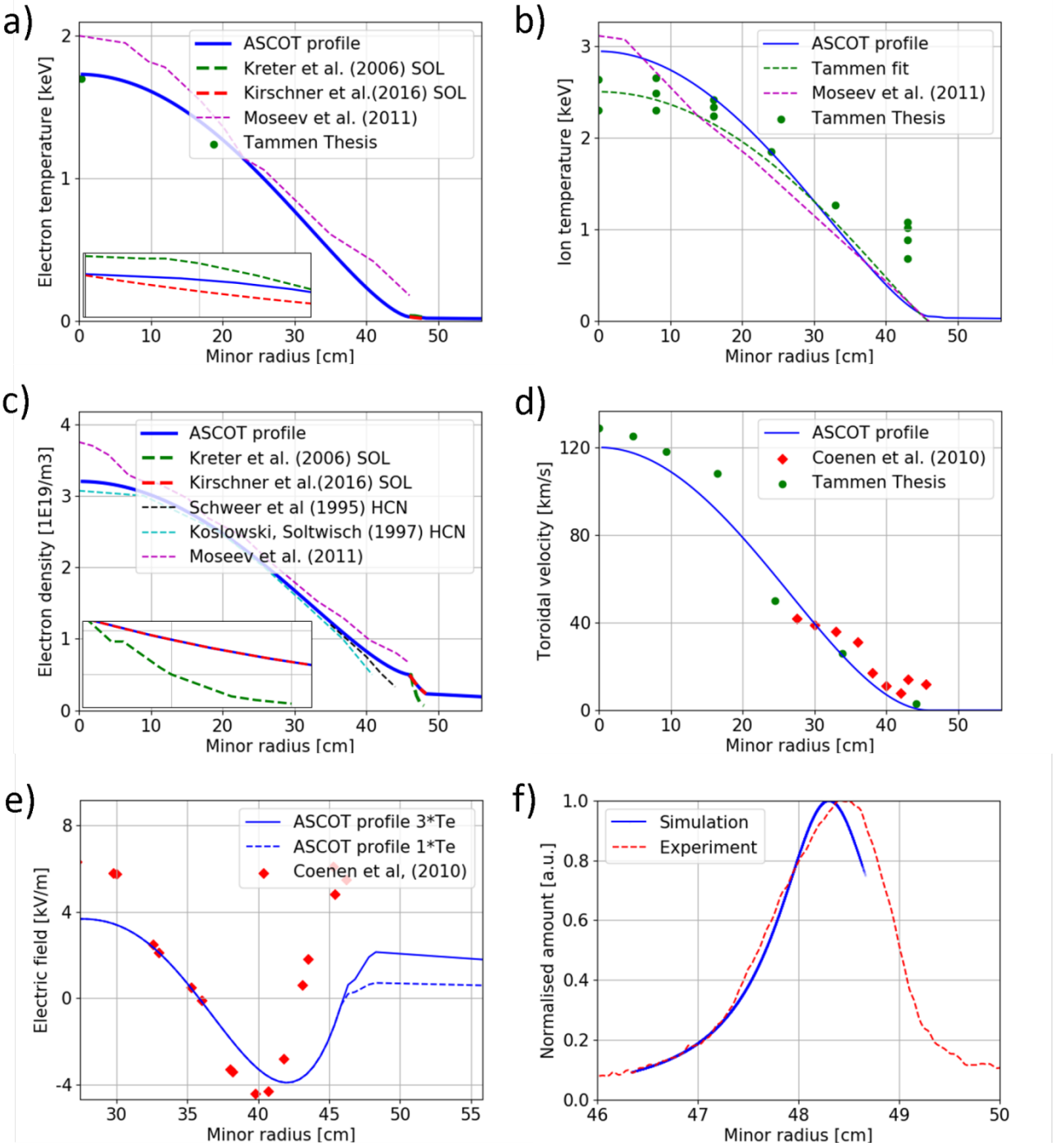

Figure 3: Simulations (IV) and (V). Influence of the toroidal plasma rotation within the LCFS is non-existent. The “stripe”-like deposition along the x=0 position is an interpolation artefact. The concentration is in arbitrary units.

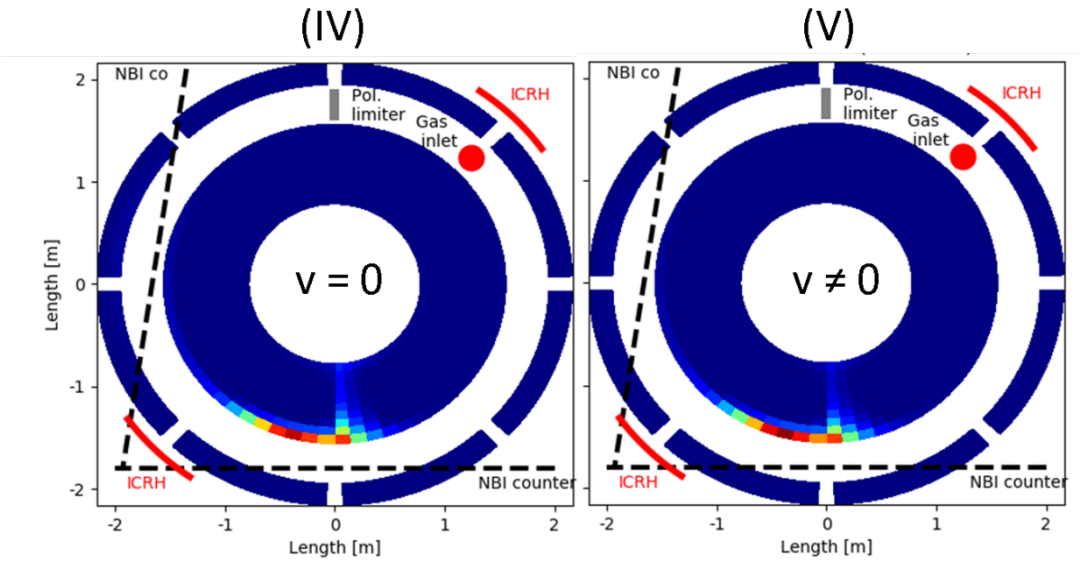

Figure 4: Simulations (VI) and (VII). Influence of the radial electric field is large because of the resulting $\vec{E} \times \vec{B}$ drift. The impact of toroidal plasma rotation stays low. The concentration is in arbitrary units.

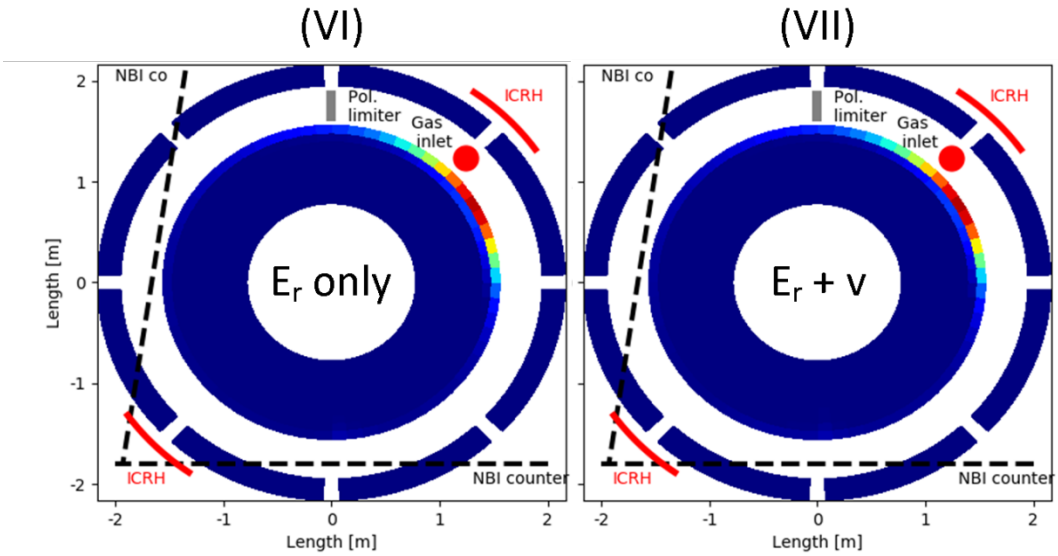

Figure 5: Simulations (VIII) and (IX). Influence of the marker starting energy on the deposition pattern is modest, causing a few degrees shift along the toroidal direction for 10 eV due to lower $\vec{E} \times \vec{B}$ drift velocity relative to overall marker velocity.

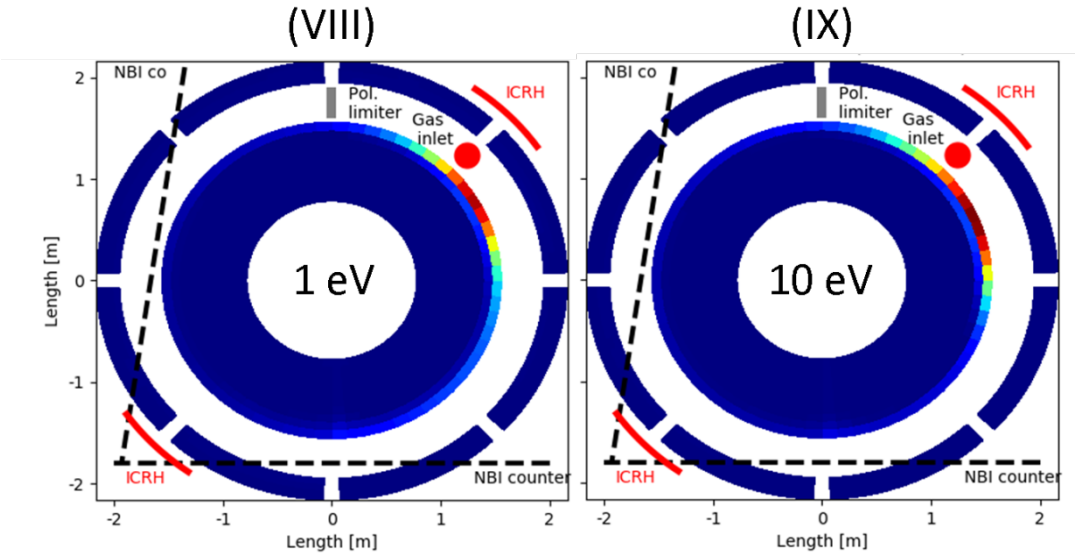

Figure 6: Simulations (X) and (X-b). Setting the electric potential in the SOL to $1T_e$ instead of 3Te decreases the poloidal movement. Extending the source from r = 46,5 cm (see Fig. 2f) to r = 44 cm gives deposition on ALT-II.

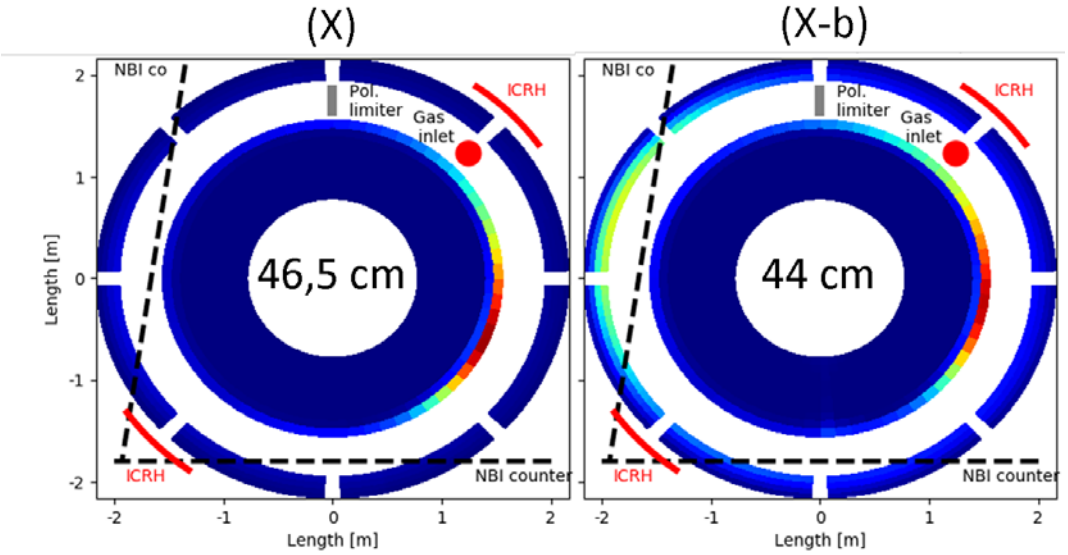

Figure 7: Simulations (XI) and (XII). No electric field also gives same deposition on the ALT-II limiter as in case (X-b) but different deposition on IBL. Realistic electric field plus "worst case" flow is rather similar to case (X) where there is no flow at all.

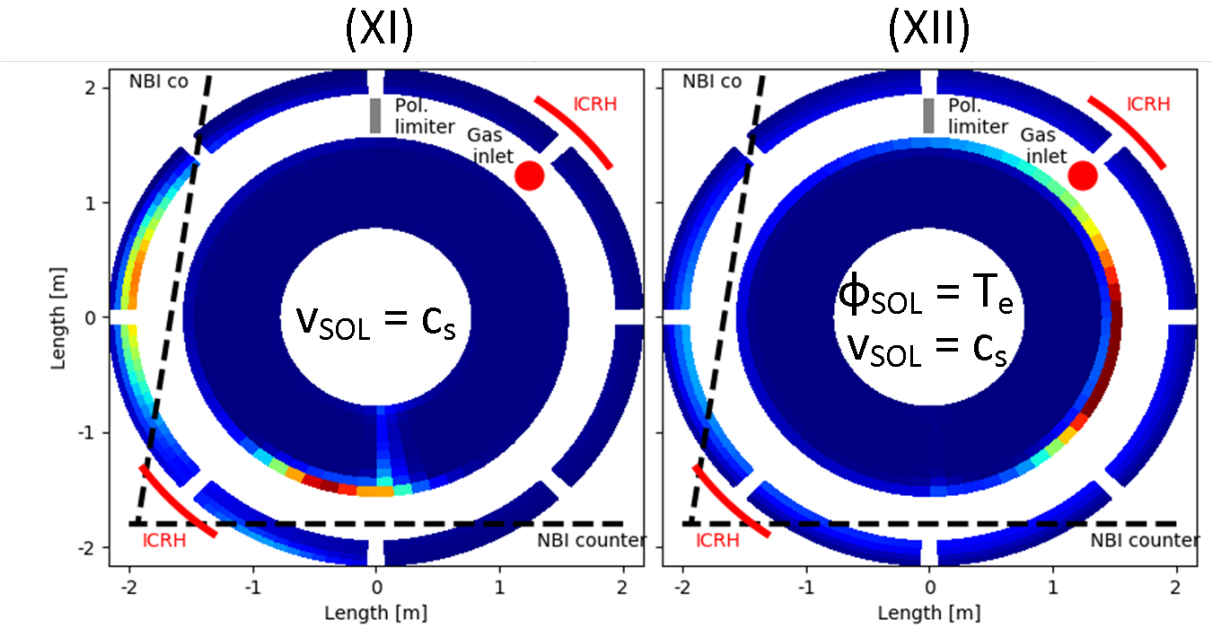

Figure 8: Simulation (XIII) and real molybdenum deposition pattern in TEXTOR, as obtained by interpolation of 571 measurement points [5]. A linear SOL profile increases Coulomb collisions close to the LCFS, enabling markers to cross the LCFS and get deposited on the ALT-II limiter.

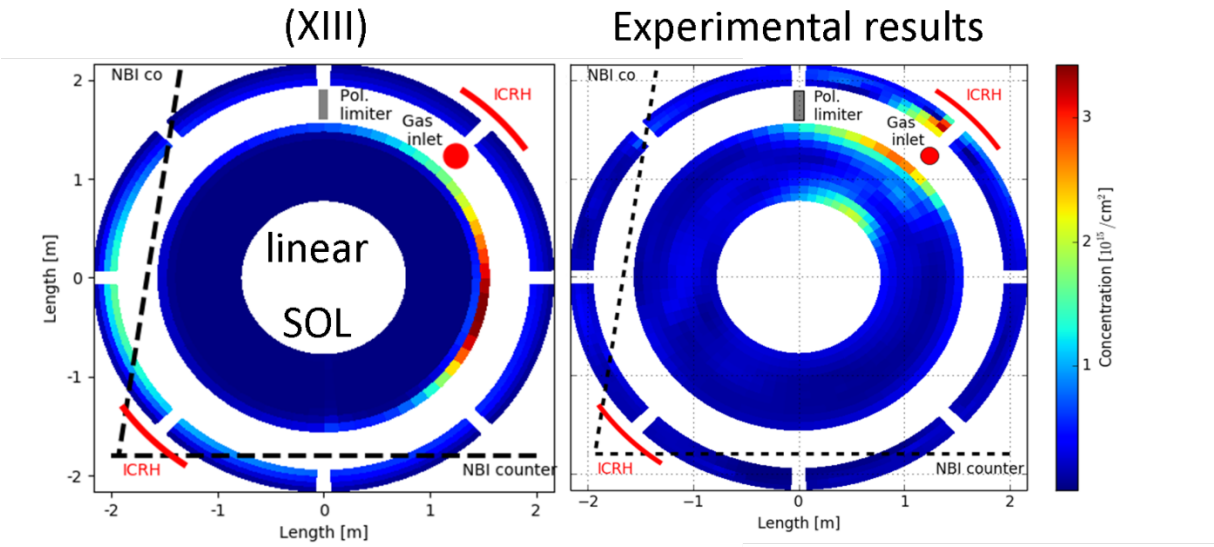

Table 1: experimental conditions for the molybdenum tracer experiment on the last operation day of TEXTOR (shots #120964 – 121007, including preparation and calibration shots).

Plasma current	350 kA
Toroidal field strength	2.25 T
Discharge duration	6 – 7 s (5 s flat-top)
Auxiliary heating	1.7 MW (co-NBI), no ICRH
MoF6 injection: - Position - Amount - No. of discharges	 Limiter Lock 1 (Fig. 1) $5.7 \cdot 10^{20}$ molecules 31 discharges with injection

Table 2: Plasma profiles used in the ASCOT simulation, with $\rho = r/a$ and a = 46 cm.

Profile	Formula
Radial electric field [V/m] (whole simulation volume)	$633 - 3962\rho + 9236\rho^2 - 9343\rho^3 + 3436\rho^4$
Bulk plasma rotation inside LCFS [km/s]	$120 \cdot (1-\rho^2)^2$
Electron temperature [eV]	$1700 \cdot (1-\rho^2)^{1.5} + 30$
Ion temperature [eV]	$T_I = 2890 \cdot (1-\rho^2)^{1.5} + 50$
Electron and ion densities [m^{-3}]	$2.7 \cdot 10^{19} \cdot (1-\rho^2)^{1.5} + 5 \cdot 10^{18}$
Radial source [cm^{-1}]	$2.977 \cdot 10^{-4} \cdot (1.876 \cdot 10^{-4} + (\rho - 1.05)^2)^{-1}$
Electron density in the SOL [m^{-3}]	$5 \cdot 10^{18} \cdot \exp(-15\frac{1}{3} \cdot (\rho - 1))$
Electron temperature in the SOL [eV]	

Table 3: overview on all the simulation cases run in this paper.

Simulation index	**I**	**II**	**III**	**IV**	**V**	**VI**	**VII**	**VIII**	**IX**	**X**	**X-b**	**XI**	**XII**	**XIII**
Atomic processes	-	X	-	X	X	X	X	X	X	X	X	X	X	X
Coulomb collisions	-	-	X	X	X	X	X	X	X	X	X	X	X	X
E(r)	-	-	-	-	-	X	X	X	X	X	X	-	X	X
$\mathbf{v_{centre}(r)}$	-	-	-	-	X	-	X	X	X	X	X	X	X	X
Source (P/R)[1]	P	P	P	P	P	P	P	R	R	R	R[#]	R	R	R
$\mathbf{E_{start}}$ **[eV]**	1	1	1	1	1	1	1	1	10	1	1	1	1	1
$\mathbf{\Phi_{SOL}(r)}$ **[T_e]**	-	-	-	-	-	3	3	3	3	1	1	-	1	1
$\mathbf{v_{SOL}(r)}$ **[c_s]**	-	-	-	-	-	-	-	-	-	-	-	1	1	-
SOL (E/L)[2]	E	E	E	E	E	E	E	E	E	E	E	E	E	L

[1] P = point source, R = radially extended source

[2] E = exponential, L = linear

[#] Radial source extends to r = 44 cm instead of 46.5 cm

Bibliography

[1] A. Weckmann, P. Petersson, M. Rubel, P. Wienhold, S. Brezinsek, J. W. Coenen, A. Kirschner, A. Kreter and A. Pospieszczyk, "Local migration studies of high-Z metals in the TEXTOR tokamak," *Physica*

Scripta, vol. T167, p. 014058, 2016.

[2] A. Weckmann, P. Petersson, A. Kirschner, P. Wienhold, S. Brezinsek, A. Kreter, A. Pospieszczyk and M. Rubel, "Whole-machine material migration studies in the TEXTOR tokamak with molybdenum," *Nuclear Materials and Energy*, vol. 12, pp. 518-523, 2017.

[3] A. Kirschner, A. Kreter, P. Wienhold, A. Weckmann, A. Pospieszczyk, R. Ding, D. Borodin, S. Brezinsek, G. Sergienko, M. Rubel, C. Linsmeier and T. Team, "Modelling of deposition and erosion of injected WF6 and MoF6 in TEXTOR," *Nuclear Materials and Energy*, vol. 12, pp. 564-568, 2017.

[4] E. Hirvijoki, O. Asunta, T. Koskela, T. Kurki-Suonio, J. Miettunen, S. Sipilä, A. Snicker and S. Äkäslompolo, "ASCOT: Solving the kinetic equation of minority particle species in tokamak plasmas," *Computer Physics Communications*, vol. 185, pp. 1310-1321, 2014.

[5] A. Weckmann, "Material migration in tokamaks: Erosion-deposition patterns and transport processes," KTH Royal Institute of Technology, Stockholm, 2017.

[6] J. A. Heikkinen, S. K. Sipilä and T. J. H. Pättikangas, "Monte Carlo simulation of runaway electrons in a toroidal geometry," *Computer Physics Communications*, vol. 76, no. 2, pp. 215-230, 1993.

[7] W. Press, B. Flannery, S. Teukolsky and W. Vetterling, Numerical Recipes: The art of Scientific Computing, Cambridge: Cambridge University Press, 1986.

[8] H. Summers, "The ADAS User Manual," The ADAS Project, 2004. [Online]. Available: http://www.adas.ac.uk. [Accessed 10 July 2018].

[9] J. Coenen, B. Schweer, M. Clever, S. Freutel, O. Schmitz, H. Stoschus, U. Samm, B. Unterberg and T. team, "Charge exchange recombination spectroscopy on a diagnostic hydrogen beam - measuring impurity rotation and radial electric field at the tokamak TEXTOR," *Journal of Physics B: Atomic, Molecular and Optical Physics*, vol. 43, p. 144015, 2010.

[10] H. F. Tammen, *The ion velocity distribution of tokamak plasmas: Rutherford Scattering at TEXTOR*, Utrecht, 1995.

[11] D. Moseev, F. Meo, S. Korsholm, T. Koskela, M. Albergante, O. Asunta, H. Bindslev, A. Bürger, V. Furtula, M. Y. Kantor, F. Leipold, P. Michelsen, S. Nielsen, M. Salewski, O. Schmitz, M. Stejner, E. Westerhof and T. team, "Comparison of measured and simulated fast ion velocity distributions in the TEXTOR tokamak," *Plasma Physics and Controlled Fusion*, vol. 53, p. 105004, 2011.

[12] A. Kreter, D. Borodin, S. Brezinsek, S. Droste, T. Hirai, A. Kirschner, A. Litnovsky, M. Mayer, V. Philipps, A. Pospieszczyk, Y. Sakawa, U. Samm, O. Schmitz, G. Sergienko, T. Tanabe, Y. Ueda, P. Wienhold and T. team, "Investigation of carbon transport by 13CH4 injection through graphite and tungsten test limiters in TEXTOR," *Plasma Physics and Controlled Fusion*, vol. 48, pp. 1401-1412, 2006.

[13] H. Koslowski and H. Soltwisch, "Electron density and q profile measurements with the far-IR interferometer-polarimeter on the TEXTOR tokamak," *Fusion Engineering and Design*, Vols. 34-35, pp. 143-150, 1997.

[14] E. Hintz and B. Schweer, "Plasma Edge Diagnostics by Atomic Beam Supported Emission Spectroscopy - Status and Perspectives," *Plasma Physics and Controlled Fusion*, vol. 37, pp. 87-101, 1995.

[15] D. L. Hildenbrand, "Thermochemical studies of the gaseous lower-valent fluorides of molybdenum," *The Journal of Chemical Physics*, vol. 65, no. 2, pp. 614-618, 1976.

[16] A. Kreter, S. Brezinsek, T. Hirai, A. Kirschner, K. Krieger, M. Mayer, V. Philipps, A. Pspieszczyk, U. Samm, O. Schmitz, B. Schweer, G. Sergienko, K. Sugiyama, T. Tanabe, Y. Ueda, P. Wienhold and T. team, "Effect of surface roughness and substrate material on carbon erosion and deposition in the TEXTOR

tokamak," *Plasma Physics and Controlled Fusion*, vol. 50, no. 9, 2008.

[17] J. P. Freidberg, Plasma physics and fusion energy, Leiden Cambridge University Press, 2007.